



A novel molecular communication inspired detection method for the evolution of atherosclerosis

Yue Sun^{a,c}, Meiling Liu^a, Yue Xiao^a, Yifan Chen^{b,c,*}

^a School of Mechanical and Electrical Engineering, Chengdu University of Technology, Chengdu 610059, China

^b Yangtze Delta Region Institute (Huzhou), University of Electronic Science and Technology of China, Huzhou, China

^c School of Life Science and Technology, University of Electronic Science and Technology of China, Chengdu 611731, China

ARTICLE INFO

Article history:

Received 18 October 2021

Revised 8 March 2022

Accepted 11 March 2022

Keywords:

Atherosclerosis

Early detection

Molecular communication

COMSOL Simulation

ABSTRACT

Background and objective: Atherosclerosis is a leading cause of potentially serious cardiovascular diseases such as heart attack, stroke, and peripheral artery disease. Due to the prolonged and non-reversible process of thickening arteries walls, atherosclerosis plaques in the blood vessels are formed that restrict the blood flow. Early detection plays a vital role in minimizing the risk as there is no reliable method to detect the early stage of the disease. This paper proposes a novel atherosclerosis detection method based on the emerging paradigm of molecular communications. The work could pave the way to implement a low-cost and straightforward early detection method of atherosclerosis in the future.

Methods: We used COMSOL to model the physical field, coupled the fluid module and the fluid particle tracking module, and mapped the contrast agent into nanoparticles (NPs). The NPs are released at the entrance of the blood vessel and received at the exit of the blood vessel, while NPs are propagating through different arterial stenosis. The arrival probability of NPs is defined as the ratio of the number of NPs that reach the outlet to the total number of released NPs. As a result of atherosclerosis, the arrival probability of NPs is affected by the dynamic flow nature changes, thereby reflecting the arterial stenosis degree. Furthermore, we introduce the multi-release method in this study, which has a similar concept of Inter-symbol interference in traditional communication. This multi-release method leads the overlapping concentrations of NPs remaining in the vessels and enhances the differences of arrival probability in different degrees of stenosis, which increases the chance of more observable results.

Results: The assessment of arterial stenosis degree can be from the early stage to the late stage of the disease. To evaluate the arterial stenosis degree, we analyzed the Poincaré maps, representing the arrival probability of NPs at different arterial stenosis. Moreover, we could directly use data to quantify the pathological process at various stages. The difference between the data results obtained through multiple release methods is more prominent than a single-released method.

Conclusions: This research proposes a new atherosclerosis detection method based on molecular communication, that is, to evaluate the arterial stenosis degree by modelling and using statistical data of NPs emission and reception in blood vessels. This method can not only use a simple method to detect the early stage of the disease. In addition, we can directly use data to quantify the pathological process of each stage, which is straightforward to assist doctors and may reduce the labour cost of traditional detection.

© 2022 Elsevier B.V. All rights reserved.

1. Introduction

Cardiovascular diseases (CVDs) are the number one non-communicable diseases worldwide, responsible for around 17.9 million deaths in 2016 [1]. Nearly half of CVD related coronary

artery disease causes deaths [2]. As one of the coronary artery diseases, atherosclerosis is defined as a decrease in blood supply to the heart muscle due to atherosclerotic plaque occlusion. The ageing population, coupled with the modern lifestyle that increases the risk factors of CVDs, such as hypertension, diabetes, obesity, tobacco use, lack of physical activity, and unhealthy diet, are the reasons behind these shocking statistics [3].

The pathological processes associated with atherosclerosis include lipid deposition under the endothelium, thickening of

* Corresponding author.

E-mail address: yifan.chen@uestc.edu.cn (Y. Chen).

the intima, smooth muscle cell proliferation, and plaque formation [4]. During the initial stages of atherosclerosis, low-density lipoprotein(LDL)-cholesterol is excessively accumulated in the acellular layer between endothelial cells and connective tissue. Here, LDL is oxidized and absorbed by macrophages through phagocytosis [4]. When macrophages are filled with oxidized LDL-cholesterol, they release some paracrine substances, attracting smooth muscle cells to these areas, leading to the formation of lipid bands. Then, the newly formed cells in the mesangium begin to migrate towards the intima and form some fibrous extracellular matrix. As cholesterol continues to accumulate, fibrous scar tissue forms around the cholesterol. Migrating smooth muscle cells also divide, and the intima begins to thicken. Intimal hyperplasia is a chronic response of vascular tissue to local blood flow that may lead to vascular occlusion.

Various substances, including lipids and connective tissue, are gradually accumulated near the vessel wall, resulting in the decrease in the cross-section of vessels used for blood supply and nutrients exchange [5]. Thus, the stage of atherosclerosis could approximately be distinguished by the degree of arterial stenosis (ASD). In severe cases, it will decrease the flow rate, form a turbulent flow, and reduce the blood supply, resulting in the downstream tissues and blood cells being destroyed due to a lack of oxygen and nutrients. Although the most common consequences are coronary heart disease and stroke, the decrease in blood supply can affect almost any organ. Atherosclerosis is vital in CVDs; however, the early detection of atherosclerosis remains a significant challenge.

Characterized by the slow thickening of the arterial walls, atherosclerosis is a prolonged and poorly perceptible process over decades. This prolonged course provides an opportunity for early detection before symptoms appear [6]. Indeed, the advances in imaging approaches have contributed to the clinical diagnosis and detection of atherosclerosis in the past; however, the advanced atherosclerotic disease could not be observed until 15 years ago [6].

According to Shepherd et al. [7], CT angiography and magnetic resonance angiography are the most accurate noninterventional diagnostic modalities for the advanced stage of artery stenosis, but no evidence to support early detection. In clinical applications, the biomarkers are employed to mark the stages by the accumulated reactions of different biological tissues. For instance, according to Uchida et al. [5], two bio-markers, Silius red dye (SR) and Fast green dye (FG), are used to detect collagen subtypes, which indicate the stages of atherosclerosis; however, it is an interventional diagnostic method. In [8], it reveals the disease-relevant transcriptional signatures by lineage imaging tracing of vascular smooth muscle cells in healthy and diseased blood vessels. As a new strategy for theranostic atherosclerosis, nanoparticles (NPs) for CVDs have attracted much attention since 2008 [2]. The application of NPs in atherosclerosis has focused on the effectiveness of contrast agents used in conventional imaging techniques to improve visualization [9]. Later on, several multi-functional imaging nano-systems have been developed, such as positron emission tomography(PET)-CT and MRI-fluorescence [10,11].

The early detection is beyond the capability of available imaging techniques that can only detect visible morphological changes in blood vessels [5]. This paper aims to provide microscopic NP dynamics in blood flow associated with the molecular communication (MC) approach. We introduce a novel early detection method to allow the whole evolution stages. This particular MC scenario emerges from the current research in the medical field of CVDs and NP dynamics in blood flow. We consider the angiography imaging with contrast agent NPs. The released NPs burst in the blood vessel, and the subsequent Poincaré maps measure the arrival probability of its downstream cross-section. The blood vessels

with protrusions correspond to the specific communication channels. Inter-symbol interference (ISI), which corresponds to the previously released particles remaining in the blood vessel, could be employed to reflect the channel features.

Subsequently, a multiple-release method is introduced to enhance the differences in the arrival probability of NPs regarding different ASD degrees. Therefore, we propose a quantitative detection method for the evolution process of atherosclerosis, which has great practical significance.

The significant contributions of this paper are summarized below: Firstly, this paper proposed an MC-inspired NPs dynamic COMSOL simulation to model the evolution of atherosclerosis. Secondly, we introduce a multi-released method that cooperates with the detection algorithms providing quantitative indicators to estimate ASD, which could assist the doctor in diagnosing the early-stage pathological process.

Finally, the rest of the paper is organized as follows. In Section 2, we present the fluid model. Then, an MC-inspired detection method is proposed in Section 3. Subsequently, Section 4 provides the simulation results and discussion. Finally, the conclusion is given in Section 5.

2. Blood flow model

The flow-based MC [12–14], which implements fluid flow for information molecules transmission, has drawn noticeable attention in recent years. However, as noted by Wicke et al. [14], it is inappropriate to apply such simplified diffusion with flow drift model in typical molecular communication application scenarios in blood vessels or microfluidic channels since the flow is far from uniform in a microscope. Therefore, investigating the blood flow model is a continuing concern within NPs application of molecular communication in blood vessels.

The fluid viscosity is related to the rate of deformability. The fluid shear stress τ represents the shear force per unit area, and the velocity gradient $\frac{\partial u}{\partial y}$ is called the shear strain rate. According to Mejia [15], under a specific range of shear strain rates, the relationship between fluid viscosity, shear stress, and shear strain rate is shown as below:

$$\tau = \mu \frac{\partial u}{\partial y}, \quad (1)$$

where μ is the dynamic viscosity.

A fluid with a constant viscosity is defined as a Newtonian fluid. As a result, the relationship between shear strain rate and viscous shear stress can be represented by a straight line passing through the origin with slope μ . While in the non-Newtonian fluid, with a time-variant viscosity, the shear stress is not proportional to the shear strain rate. Blood flow, regarded as an incompressible fluid that deforms continuously under the shear force, is a non-Newtonian fluid with the influence of aggregation of blood cells, such as red blood cells and white blood cells. According to hemorheology [16], blood exhibits non-Newtonian fluid behaviour at low flow shear strain rate. Thus, the blood behaves as a Newtonian fluid in the region with a relatively high shear strain rate. Moreover, the flow shear strain rate is very high in the macrovascular and artery. Consequently, blood flow in the artery behaves as a Newtonian fluid since the aortic flow has a much higher shear strain rate.

The Reynolds numbers, which distinguish the laminar and turbulent flow, are often used to predict stenosis and thrombosis due to flow-induced stress on blood elements in the cardiovascular system [17]. Inertial and viscous forces determine the fluid. Particularly, with a low Reynolds number, the flow dominated by the viscous force is called a laminar flow, while the Reynolds number higher than 2320 [18], the flow gradually becomes turbulent.

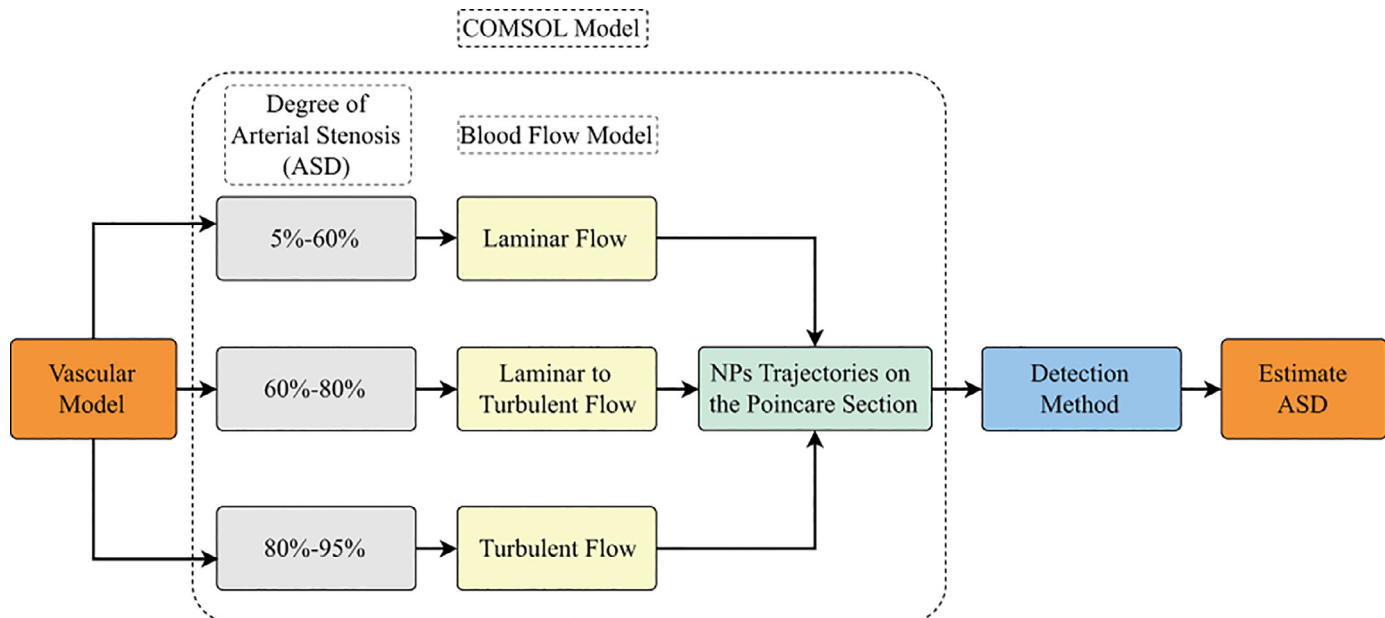


Fig. 1. Illustration of the system model.

For diseases with degrees of atherosclerosis, the impact of the viscosity of blood on hemodynamics could be much more complicated than in a vessel without disease, since stenosis in an arterial vessel segment, resulting in significant reductions of the cross-sectional area of the vessel and subsequent changes in the instantaneous Reynolds number [19]. During systole, the left ventricle generates pressure, which is conveyed outward via waves and the flexibility of the arteries. The aortic valve opens when the pressure in the left ventricle (upstream) surpasses that in the aorta (downstream), allowing blood to flow out of the heart. The pressure distribution in blood arteries and the velocity distribution of the transition from laminar to turbulent flow are also affected by fluid pulsation. Based on the instantaneous Reynolds number in the ascending aorta, the flow will be turbulent for much of the systolic phase due to the quick increase in flow velocity during early contraction. In the initial stage, however, [20] claims that blood flow in the aorta remains laminar and well-streamlined since the accelerated contraction tends to maintain the flow stable. The reverse development of the pressure gradient during flow deceleration causes flow disturbance at the late contraction stage. However, within a cardiac cycle, the flow instability interval, middle and late contraction, is very short (about 150ms) [20], and the diastolic stage is as follows, with the low velocity and low instantaneous Reynolds number. As diastole begins, the flow will be stabilized once more by a new acceleration phase. The impact of blood viscosity on the overall pressure drop across the arterial is significant at a low Reynolds number of 100 or less [19].

The evolution of atherosclerosis changes the dynamic nature of blood flow due to stenosis. Hence, As the ASD increases, the blood flow transition phase from laminar to turbulent. This paper thereby implements laminar flow, the transition phase, and turbulent flow models regarding ASD, from 5% to 60%, from 60% to 80%, and 80% to 95% respectively. As seen in Fig. 1, it illustrates the logic flow of the system, which includes COMSOL simulations and detection methods.

In healthy or early-stage atherosclerosis, blood flow with a low Reynolds number in the flow can thus be modelled as laminar flow, discussed in Section 2.1. In the transition phase, specifically, during the deceleration of systole, blood flow in the ascending aorta may be slightly interrupted. Nevertheless, the period is usu-

ally too short for blood to produce fully developed turbulence. However, as the ASD increases, the laminar blood flow gradually becomes turbulent, such as downstream artery stenosis. Finally, the flow is fully turbulent in the advanced stage, and the turbulent flow model is illustrated in Section 2.2.

2.1. Laminar flow model

The laminar blood flow in the blood circulatory system can be described by the Navier-Stokes equation and the continuity equation of incompressible fluid, respectively, as follows [16]:

$$-\nabla p + \rho \mathbf{g} + \mu \nabla^2 \mathbf{v} = \rho \frac{D\mathbf{v}}{Dt}, \quad (2)$$

$$\nabla \cdot \mathbf{v} = 0, \quad (3)$$

where p is the blood pressure, ρ is the fluid density, μ is the dynamic viscosity, \mathbf{g} is the gravity coefficient, and \mathbf{v} is the fluid velocity. The vector operator ∇ is defined as

$$\nabla = i \frac{\partial}{\partial x} + j \frac{\partial}{\partial y} + k \frac{\partial}{\partial z}, \quad (4)$$

and $\frac{D}{Dt}$ is defined as [21]

$$\frac{D}{Dt} = \frac{\partial}{\partial t} + u \frac{\partial}{\partial x} + v \frac{\partial}{\partial y} + w \frac{\partial}{\partial z}, \quad (5)$$

which denotes the time derivative of a physical quantity moving with the fluid particle.

The NP trajectory is calculated by solving the second-order motion equation of the position vector component of NP from Newton's second law,

$$\frac{dx}{dt} = \mathbf{v}, \quad (6)$$

$$\frac{d}{dt} (m_p \mathbf{v}) = \mathbf{F}_t, \quad (7)$$

where x is the position of the particle, v is the particle velocity, m_p is the mass of the particle, and F_t is the total force. It is applicable to Stokes's law since the size of the particle is small, and the speed

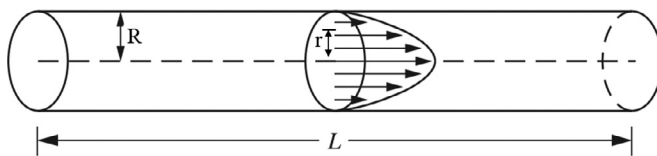


Fig. 2. Illustration of parabola shaped velocity profile of laminar flow.

relative to the fluid is not large, the Stokes drag law is applicable, according [20]:

$$F_D = \frac{1}{\tau_p} m_p (u - v), \quad (8)$$

where F_D is the sum of the drag force on a particle sinking in a fluid, u is the velocity of the surrounding fluid, v is the particle velocity, and τ_p is the particle velocity response time:

$$\tau_p = \frac{\rho_p d_p^2}{18\mu}, \quad (9)$$

where ρ_p is the particle density and d_p is the particle diameter.

The velocity profile of laminar flow is a parabola shape, shown as in Fig. 2, presented by the Hagen-Poiseuille equation [12], which is derived from the Navier-Stokes equation:

$$v(r) = \frac{1}{4\mu} \frac{\Delta p}{L} (R^2 - r^2), \quad (10)$$

where $v(r)$ is the velocity profile, L is the length of the vessel, R is the radius of the vessel, r is the distance from the longitudinal axis of the vessel, and Δp is the pressure drop along a vessel. The flow velocity declines to zero as r increases to R and reaches the vessel wall.

The pressure drop in (10) is derived from the modified Bernoulli equation as follows:

$$\Delta p = K_L \left(\rho \frac{v^2}{2} \right), \quad (11)$$

where Δp is the pressure drop, $K_L \approx 0.04$ at the entrance, and $K_L \approx 1.0$ at the exit area. As for the turbulent flow, the pressure drop can be measured by the energy dissipation caused by reflux.

2.2. Turbulent flow model

The blood flow of the ascending aorta will be slightly disturbed during the deceleration of the systole, but it is insufficient to transform the blood flow into a turbulent flow. However, a laminar flow becomes a turbulent flow at the downstream or the remote area due to the stenosis caused by atherosclerosis, as shown in Fig. 3. In the advanced stage of stenosis, the plaques would rupture, and the thrombus is transferred to this part, which eventually leads to blood vessel obstruction.

Unlike the Laminar flow model provided with closed-form mathematical expressions, turbulent flow is the numerical model in the COMSOL simulation. The Reynolds-Averaged Navier-Stokes (RANS) is implemented to simulate turbulence by decomposing the flow quantities into time-averaged and fluctuating components [22]. In addition, the $k - \varepsilon$ model applies the definitions of turbulence viscosity relating the turbulence dynamic k with the turbulence dissipation rate ε as below:

$$\mu_T = f \left(\frac{\rho k^2}{\varepsilon} \right) \quad (12)$$

where μ_T is defined as the turbulence viscosity, ρ is the fluid density, ε is the turbulence dissipation rate, and k is the turbulence dynamic k defined as the Kronecker delta term, which is the proportionality constant for the flow velocity squared term [22]. As for the near-wall treatment, we choose the standard wall functions.

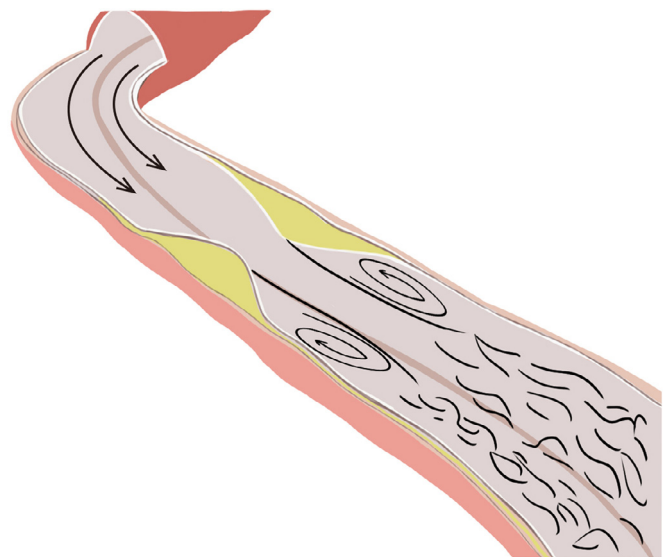


Fig. 3. In the advanced stage of stenosis, the ASD would reach 80%. The blood flow is transformed into a turbulent flow, which would do harm to both the vessel and red blood cells.

According to Rittgers and Shu [23], Chandran et al. [24], as ASD increases and reaches 40%, it forms a separate area, located between the high motion flux and vessel walls, resulting in a slow fluid velocity and a reflex behind the stenosis. Meanwhile, the reflux weakens the blood's ability to deliver oxygen and nutrients. When ASD reaches 80%, the Reynolds number is in the turbulent range. A grumble and muffled noise, called an arterial murmur [24], is generated due to stenosis, the diagnosis feature.

3. Detection method

Figure 4 shows the detection schematic. The NP motion in the blood is affected by the parameters of both particles (ratio and volume) and vessels (diameter and blood flow rate). In order to focus on the effect of vascular stenosis on the NP motion, the NPs utilized are assumed to have the same type and quantity.

In the single-release detection method, all the NPs released at the inlet at a single time without ISI, the NPs arrival probabilities at the outlet of the studied blood vessels shows little difference as the ASD increase. The simulation results of single-release detection are shown in Table 4. Therefore, we introduce a multiple-release method to enhance the affection of the blood flow to the NPs trajectory. The NPs are released every second within the study time instead of all at the beginning. This multiple-release method is inspired by the concept of ISI, where previously arrived symbols with long tails cause interference to the current signal. In MC, ISI

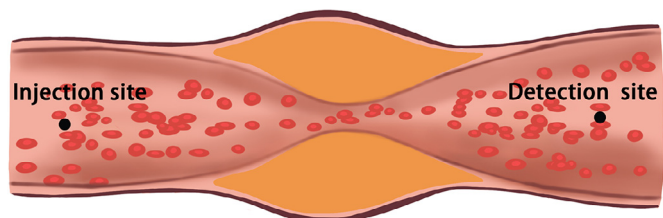


Fig. 4. Schematic of the proposed detection method. The NPs released at the injection site can be received by the detection site. Due to the effect of turbulent flow caused by stenosis, the reflux or back-flow could indicate the serious degrees of vessel stenosis.

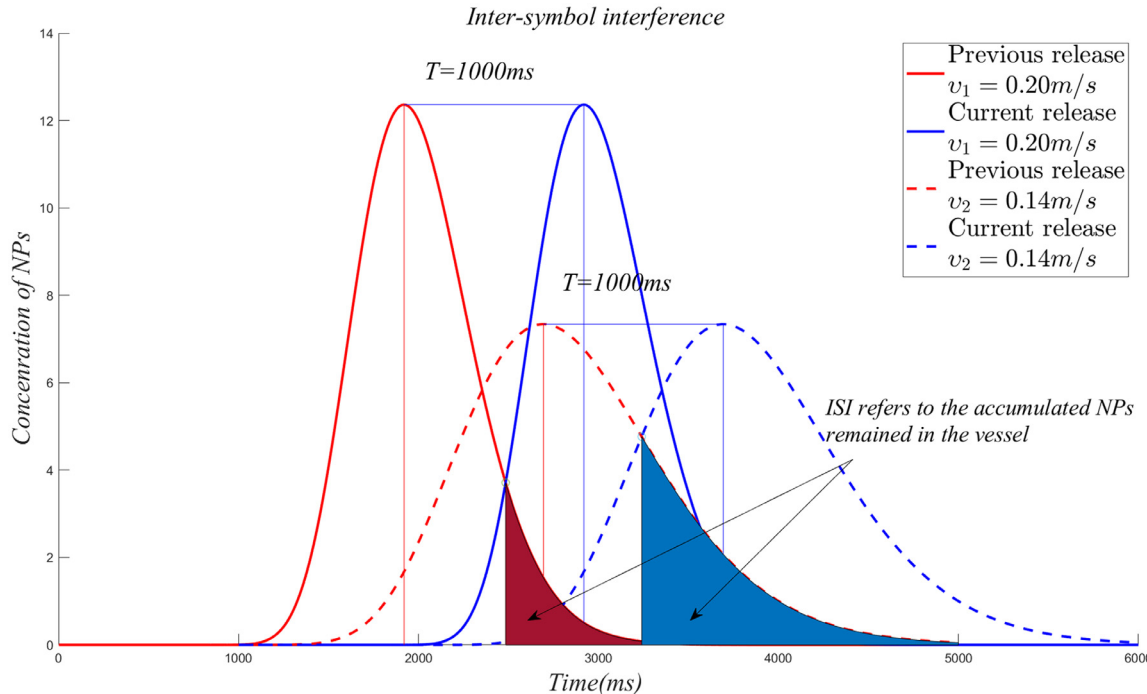


Fig. 5. Illustration of ISI in MC.

Table 1
Simulation settings.

Radius	1.5 mm
length	20 mm
ρ	1060 kg/m ³
μ	0.005 Pa · s
u	0.2 m/s
p	125.91 mm Hg
simulation time	5 sec

refers to the previously released particles that remain in the channel. However, it is different from reducing interference in the traditional communication systems but obtains more noticeable distinctive features of different blood vessels by intentionally increasing ISI. Thus, it is very different from the traditional MC systems where the desirable ISI is to be eliminated.

3.1. ISI analysis

In the laminar flow model, the propagation of NPs regarding the blood flow could be modelled by advection-diffusion equation [25]. Thus, the mass transport phenomena operated by the blood vessels for the propagation of the NPs are two, namely, advection and diffusion. As a result of advection, the NPs are subject to their translation while in suspension in the blood, which flows at different velocities in different locations of the blood vessels [26]. The velocity profile follows the Hagen-Poiseuille equation in (10). Due to diffusion, the NPs are subject to the Brownian motion spread in the blood vessel from higher to lower concentrations. The motion of NPs developed as a solution to the advection-diffusion equation [26], which indicates concentration of NPs $C(x, t)$ at the location of the blood vessel concerning blood velocity $v(r)$ as functions of the r , distance from the longitudinal axis of the vessel. It is expressed as follows:

$$\frac{\partial C(x, t)}{\partial t} = D \frac{\partial^2 C(x, t)}{\partial x^2} - v \frac{\partial C(x, t)}{\partial x} \quad (13)$$

where D is the diffusion coefficient of NPs. By solving the (13), with the boundary conditions $\lim_{x \rightarrow \pm\infty} C(x, t) = 0$ and initial condition $C(x, 0) = C_0$. In a 3D vessel, the probability density function (PDF) solution to the corresponding advection-diffusion equation is the concentration of NPs distribution [25], as follows:

$$C(x, t) = \frac{C_0}{\sqrt{4\pi Dt}} e^{-\frac{(x-vt)^2}{4Dt}} \quad (14)$$

Subsequently, the impales response of the blood vessel channel in MC shows below:

$$h(x, t) = \frac{1}{(4Dt)^{\frac{3}{2}}} e^{-\frac{(x-vt)^2}{4Dt}} \quad (15)$$

The multi-release method releases an impulse number of NPs at the start of each symbol interval. ISI affect the detection of current arrived NPs, resulting from the accumulated previous-release NPs. Unlike traditional communications with electromagnetic waves, MC can not effectively alter the shape of the arrival pulse, such that ISI is avoided. The NPs from the previous release dominate in changing the arrival probability due to the time-variant velocity of blood flow. Thus, the ISI is expressed below:

$$s_i(d, t) = \sum_{j=0}^I \frac{M}{(4Dt + jT)^{\frac{3}{2}}} e^{-\frac{(d-v(t+jT))^2}{4D(d+jT)}} \quad (16)$$

where T denotes the time interval of the former and later release, and M is the number of NPs released at one time. As seen in Fig. 5, it illustrates the impulse response of current and previously released symbols with the time interval 1sec and the shaded area indicates the ISI, accumulated NPs remained in the vessel. Additionally, the ISI increases as the flow velocity decreases. Due to stenosis at the protrusion of the vessel wall, the dynamic flow changes affect the NPs arrival probability, which is discussed in the detection method.

3.2. Detection algorithm

The number of particles that reach the outlet boundary determines the transmission arrival probability. The transmission arrival

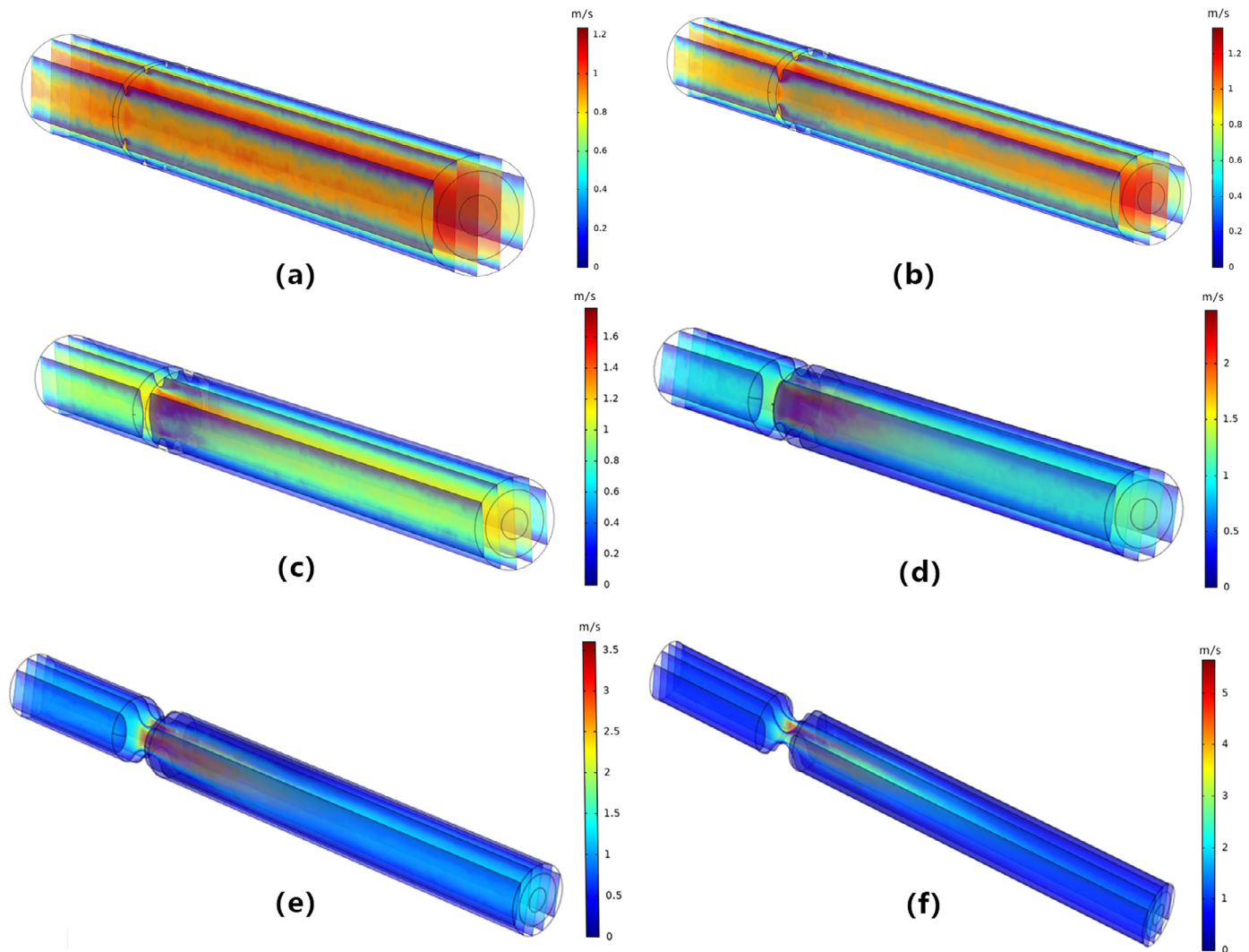


Fig. 6. (a)–(f) demonstrate the flow velocity changes when ASDs are 5%, 15%, 25%, 35%, 45% and 55%, respectively. The flow velocity near the vessel wall is often lower than that in the centre area. By comparing figures, we can see that the flow velocity shows a positive correlation with ASD. Remarkably, the blood flow may undergo an acceleration near the vicinity of the stenosis part, where the velocity could be multiple of the peak under 5% ASD, according to (d)–(f).

Table 2
The probabilities of NPs detected at the outlet under different ASDs.

5%	15%	25%	35%	45%	55%	60%
0.33033	0.27500	0.26222	0.24333	0.13611	0.093889	0.028333

probability is defined as the ratio of the number of NPs that reach the outlet to the total number of NPs released. The transmission probability for the molecular flow interface is given by the following:

$$\chi_i = \frac{\int_{\text{outlet}} (J_i - G_i) dl}{\int_{\text{inlet}} (J_i - G_i) dl} \quad (17)$$

where J_i is the outgoing flux of the i th releasing time instant, G_i is the corresponding incident flux of the i th releasing time instant, and l is the radial distance. The difference between the numerator and the denominator is due to stenosis vessels affecting the NPs obtained at the outflow interface in the denominator, resulting in particle collision or adhesion at the vessel wall. In the multiple-release method in each time, $J_i - G_i$ refers to the released particles that remain in the blood vessel, which is essential to the ISI from the MC perspective. As ISI increases, the transmission probability, χ , shows a more noticeable difference, as demonstrated in

Section 4. Therefore, the probability obtained results from the accumulation of ISI per second when the study time (5s) is over, and a significant difference can be shown to distinguish different ASD.

4. Results

4.1. Parameter setting and boundary conditions

The COMSOL simulation employs the fluid-structure coupling interface is employed in the COMSOL simulation. Simulation computation convergence is facilitated by setting the fluid velocity inlet and the fluid pressure at the outlet. The simulation parameters are based on the classic textbooks [27,28]. Longer vessels before the stenosis trend to similar results with the parameter setting in Table 1; however, there are no distinguished differences in NPs arrival probability between degrees of stenosis. In addition, if the length is too long, simulation results may fail to converge in the

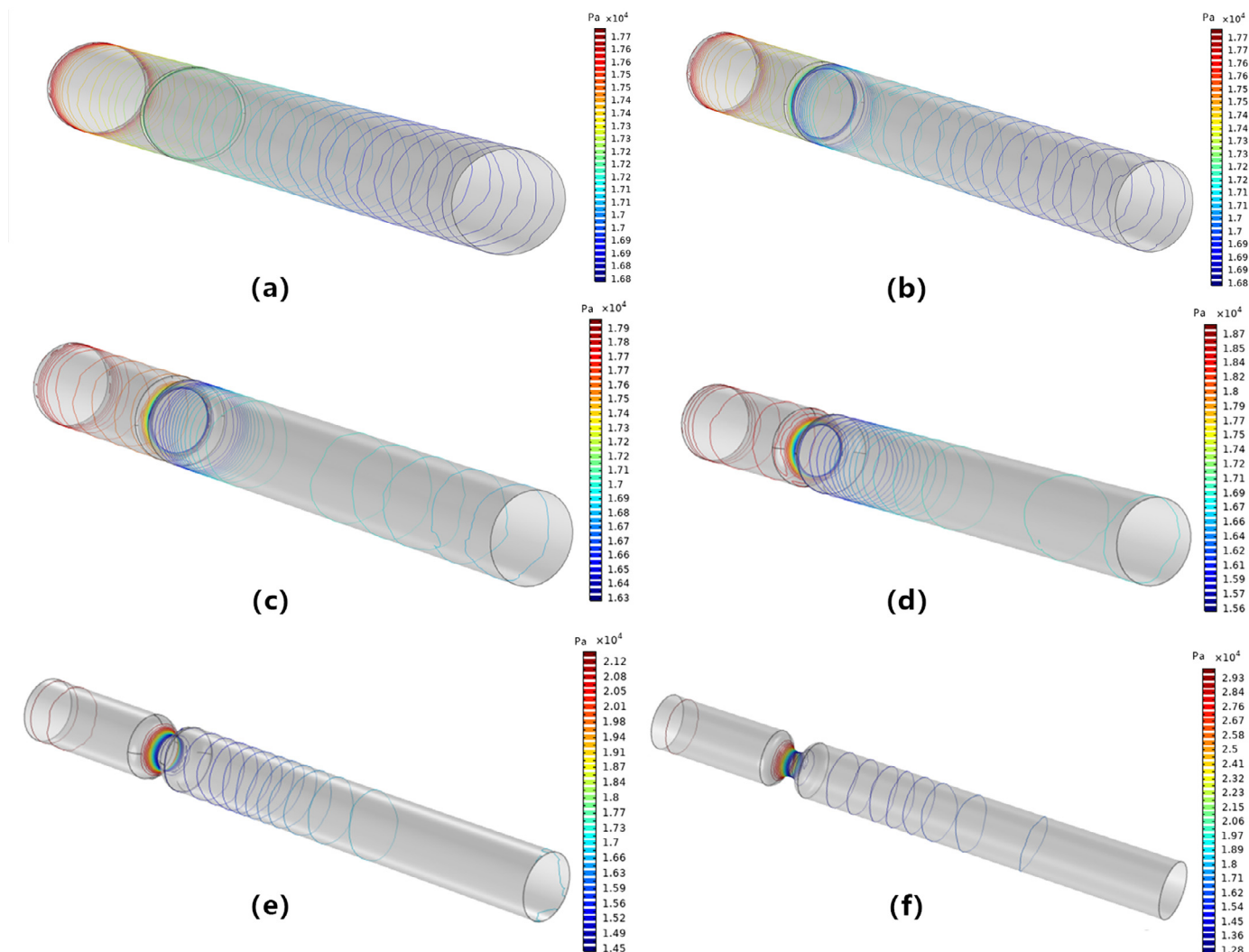


Fig. 7. Illustration of the pressure changes under ASDs ranged from 5% to 55%. When ASD increases, the high-pressure part will gradually shift to the right and concentrate on the anterior wall of the stenosis, according to (d)–(f). In addition, the pressure would reach its peak near the anterior wall, then significantly drop in the narrowest part.

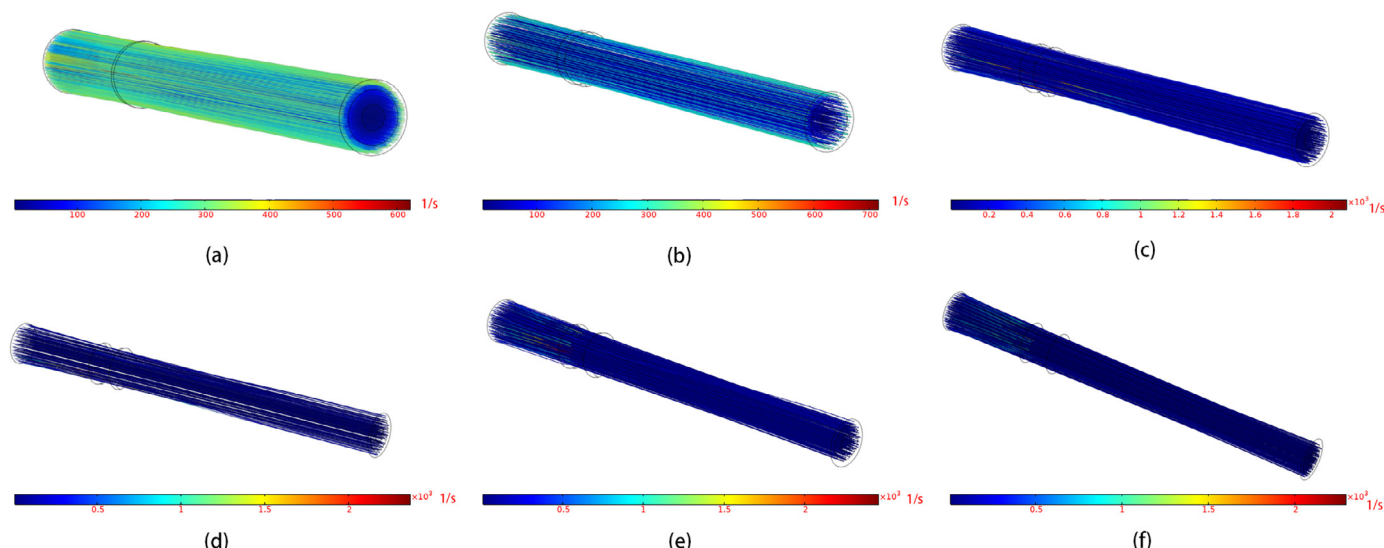


Fig. 8. The NP trajectories are determined under different ASDs. The circles at both ends represent the vascular wall, while two circles in the middle illustrate the stenotic area. As shown in (c)–(f), although the trajectory lines turn dark when ASD exceeds 25%, the NP shear rate increases significantly. Note that different graphs have different orders of magnitude. Moreover, the trajectories converge towards the centre area.

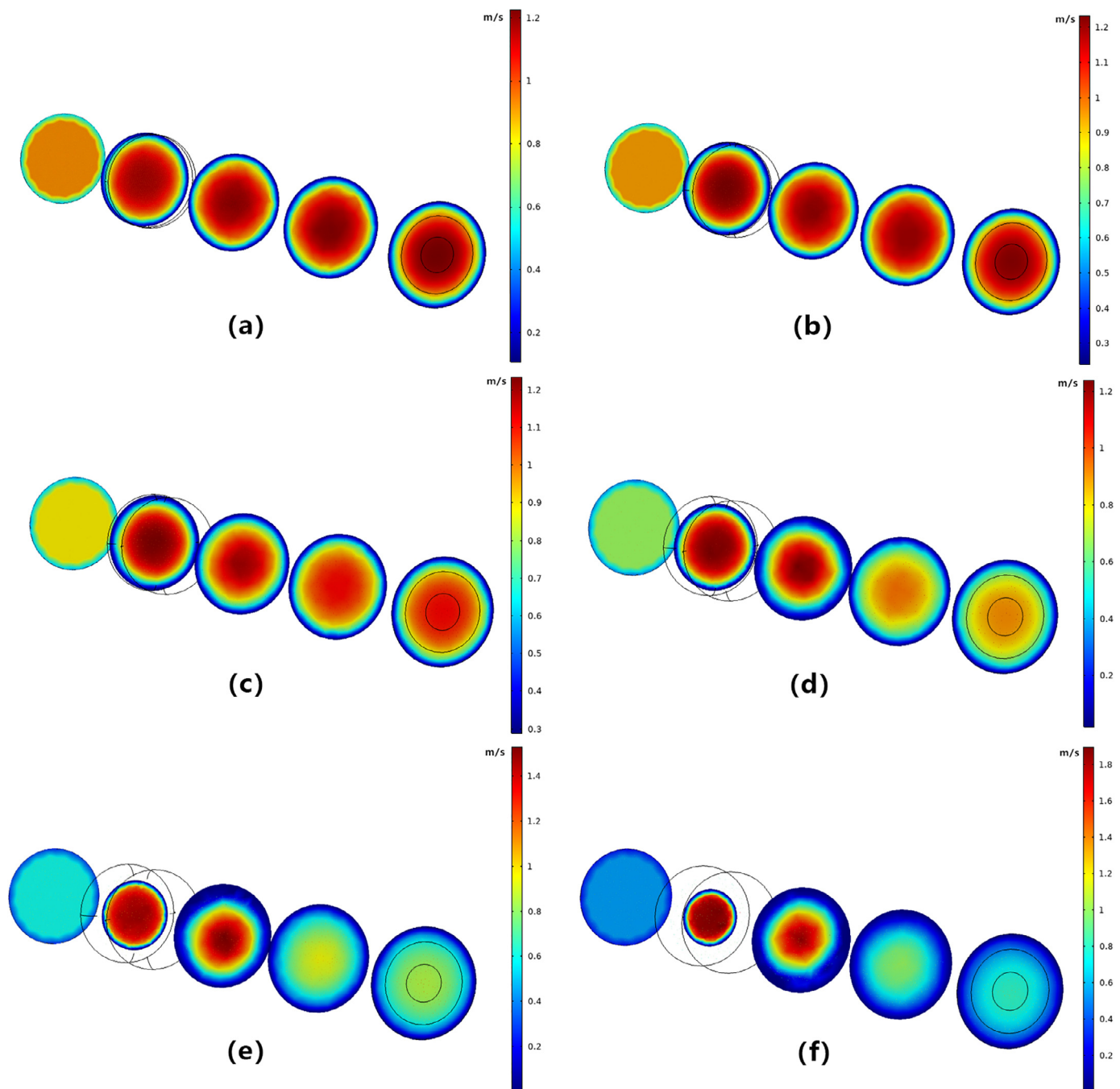


Fig. 9. Poincaré maps under various ASDs. The colour of points on each cross-section represents the probability of NPs passing through the cross-section in the simulation. As ASD increases, the NPs are more likely to assemble in the central area.

Table 3

The probabilities of NP arrival at the outlet of late stage atherosclerosis.

60%	65%	70%	75%	80%
0.16111	0.17778	0.20278	0.20000	0.052778

Table 4

The probabilities of NPs arrival without ISI.

5%	15%	25%	35%	45%	55%	60%
1	0.99967	0.98667	0.98333	0.90933	0.85867	0.81333

COMSOL. Therefore, the length is set to 20 mm, while the blood vessel radius is 1.5 mm, the fluid density ρ is 1060 kg/m³, and the dynamic viscosity μ is 0.005 Pa · s. At the inlet boundary, the fluid velocity u is 0.2 m/s, and the systolic pressure at the outlet boundary is 125.91 mmHg. In addition, the simulation time is 5 sec. All

the parameters are used in different ASD simulations, guaranteeing fair comparisons with converge results.

In the modeling simulation, we add the particle tracing for fluid flow (FPT) interface to record the trajectory of NPs. We choose the default Freeze option as the boundary condition for the vessel wall in COMSOL [29]. As for the boundary condition of the vessel wall,

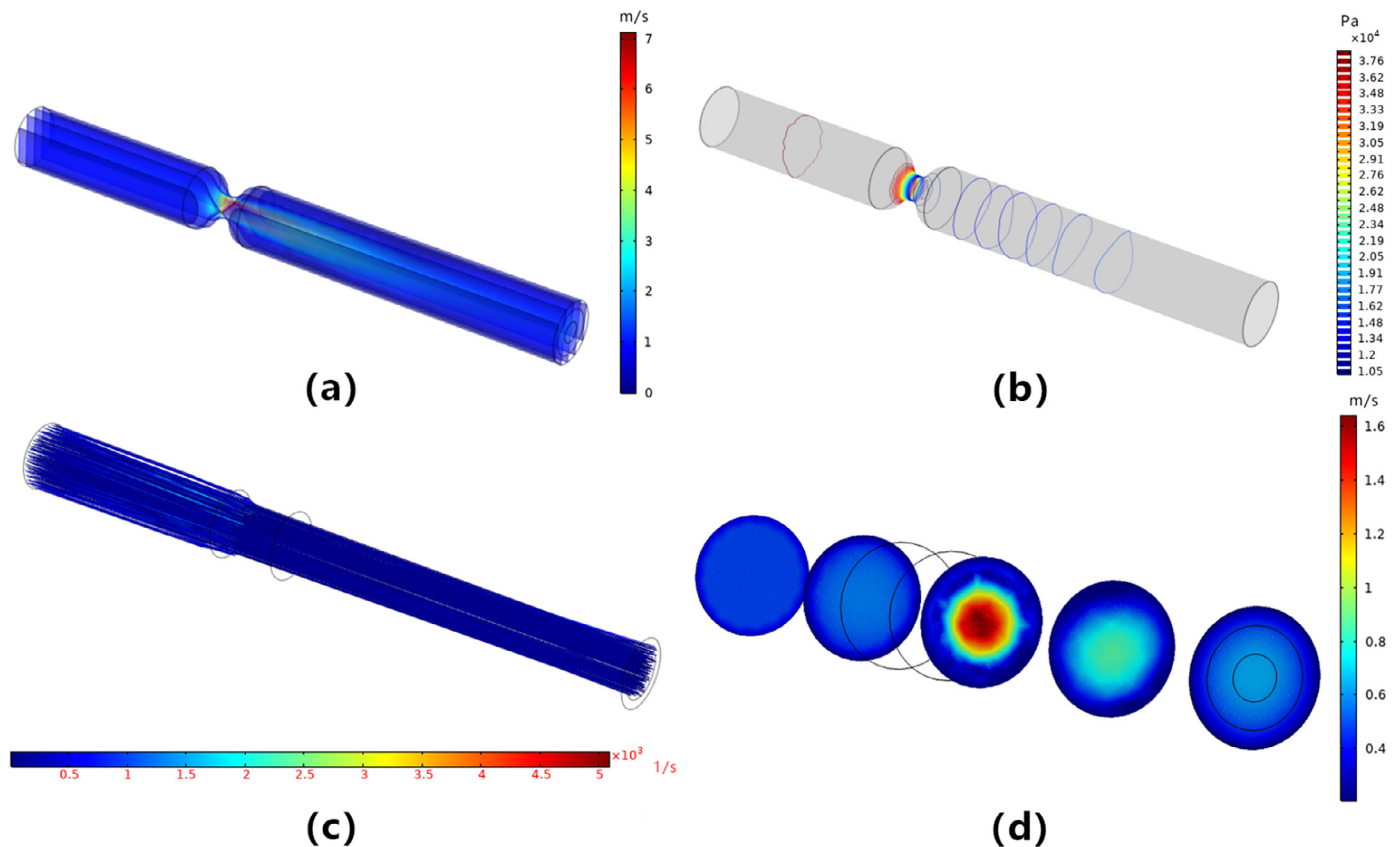


Fig. 10. (a) The fluid velocity, (b) the wall pressure, (c) the particle trajectory and (d) the Poincaré Map at 60% ASD.

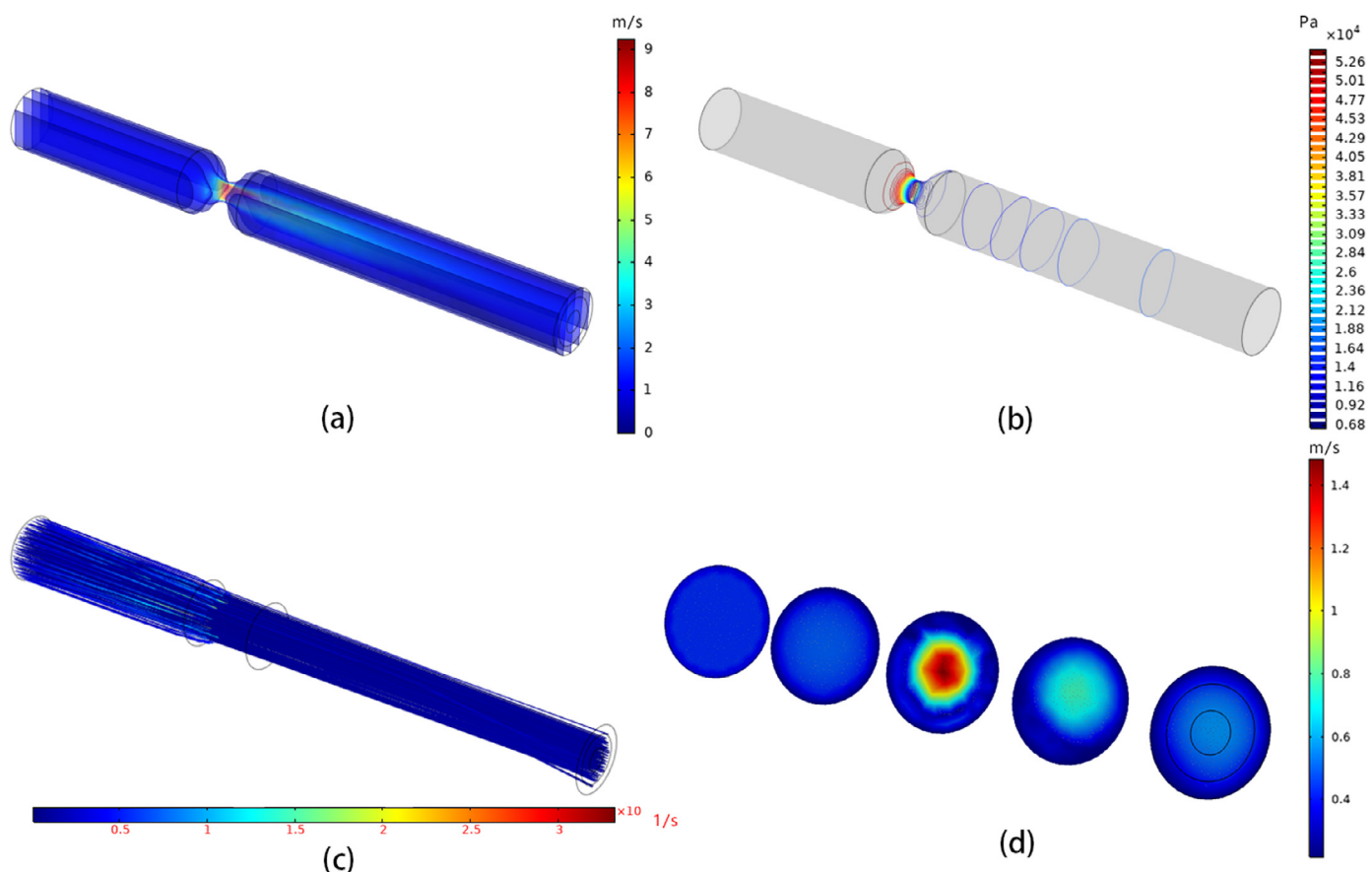


Fig. 11. (a) The fluid velocity, (b) the wall pressure, (c) the particle trajectory and (d) the Poincaré Map at 65% ASD.

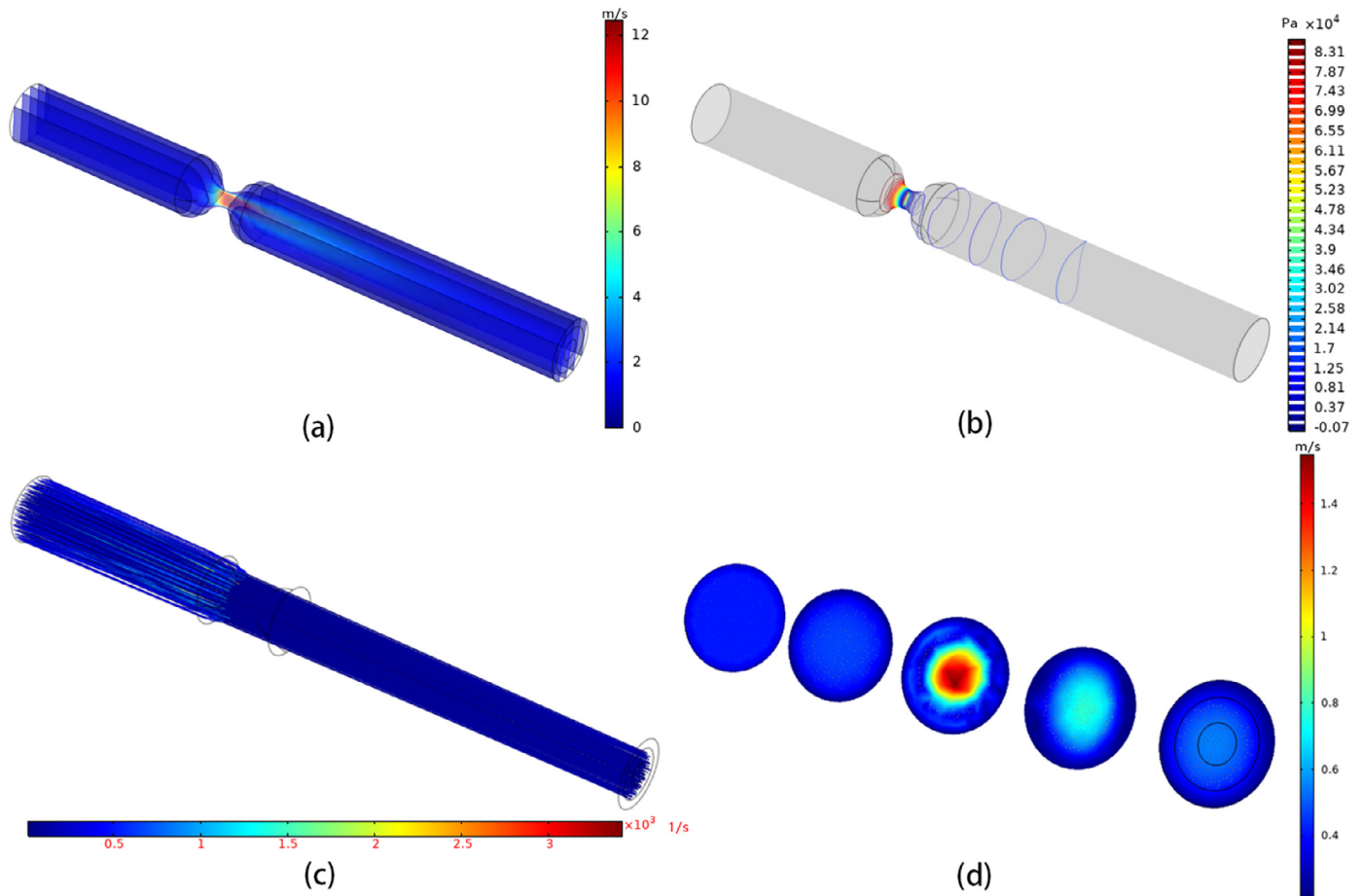


Fig. 12. (a) The fluid velocity, (b) the wall pressure, (c) the particle trajectory and (d) the Poincaré Map at 70% ASD.

Table 5

The probabilities of NPs arrival with entire outlet section.

5%	15%	25%	35%	45%	55%	60%
0.83278	0.83333	0.83333	0.91111	0.75222	0.71944	0.65556

there are nine models in COMSOL: Freeze (the default), Bounce, Stick, Disappear, Pass-through, Diffuse scattering, Mixed diffuse, Specular reflection, and General reflection. The freeze boundary condition is typically used to recover the velocity distribution of charged NPs at the instant hitting of the vessel walls, where the NPs position is no longer changes, and the velocity remains the same value as when the NP stuck the wall. In contrast, the stick option fixes the NPs position when the wall is struck and sets the velocity to zero, which is not suited for the simulation concerning velocity. Since the various substances, lipids, and connective tissue accumulate near the vessel wall with the evolution of atherosclerosis, the sclerotic vessel walls gradually lose elasticity [5]. Thus, bounce or reflection options are not suitable. Consequently, by choosing the freeze boundary condition, we could analyze the velocity of the NPs at instant contact with the protrusion vessel wall.

It is hard to obtain the distinguished arrival probabilities if the release frequency is too low. However, if the release frequency is too high, the computation results are prone to non-convergence. Thus, we set the release frequency 1Hz. The NPs are released each second to enhance the influence induced by the channel of vessels in the propagation process. For the convergence in the calculation, the number of particles released each time is 300. The particle

density is normalized according to the fluid velocity at the outlet. Specifically, the higher the inlet velocity, the more the released NPs. Due to the inertia, most particles are detected in the centre of the channel, and its probability is approximated when the stenosis level is relatively slight. The proposed solution is to detect the NP concentration in the toroidal near the vessel wall with a small radius of 11 mm.

4.2. Results discussions

According to hemodynamics [16], blood flow in a high-shear-rate artery is generally regarded as a Newtonian fluid, while the blood vessel is considered a laminar flow in early-stage atherosclerosis.

The changes in tangential velocity and vessel pressure induced by the stenosis are illustrated in Figs. 6 and 7, respectively. When blood flows through the stenosis, the velocity increases accompanied with the pressure decreases and local resistance increases [30]. As the ASD increases, the flow trend swirls and turbulence, the sudden pressure drop at the larynx is more significant and may even lead to plaque collapse. In the advanced stage of atherosclerosis, autopsy results in [5] also demonstrate that the plaque ruptured, resulting in a blood clot that migrated to the site and eventually caused a sudden blockage.

The NP trajectories in the fluid are shown in Fig. 8, where the colours of the trajectory lines indicate the NP shear rate. It can be observed that the reduction of the capable transflux area hinders NPs from passing through the stenosis. As shown in Fig. 8(c)-(f), the ASD increases from 5% to 55%, and the NPs trajectories converge towards the center area. Since the Freeze model is the

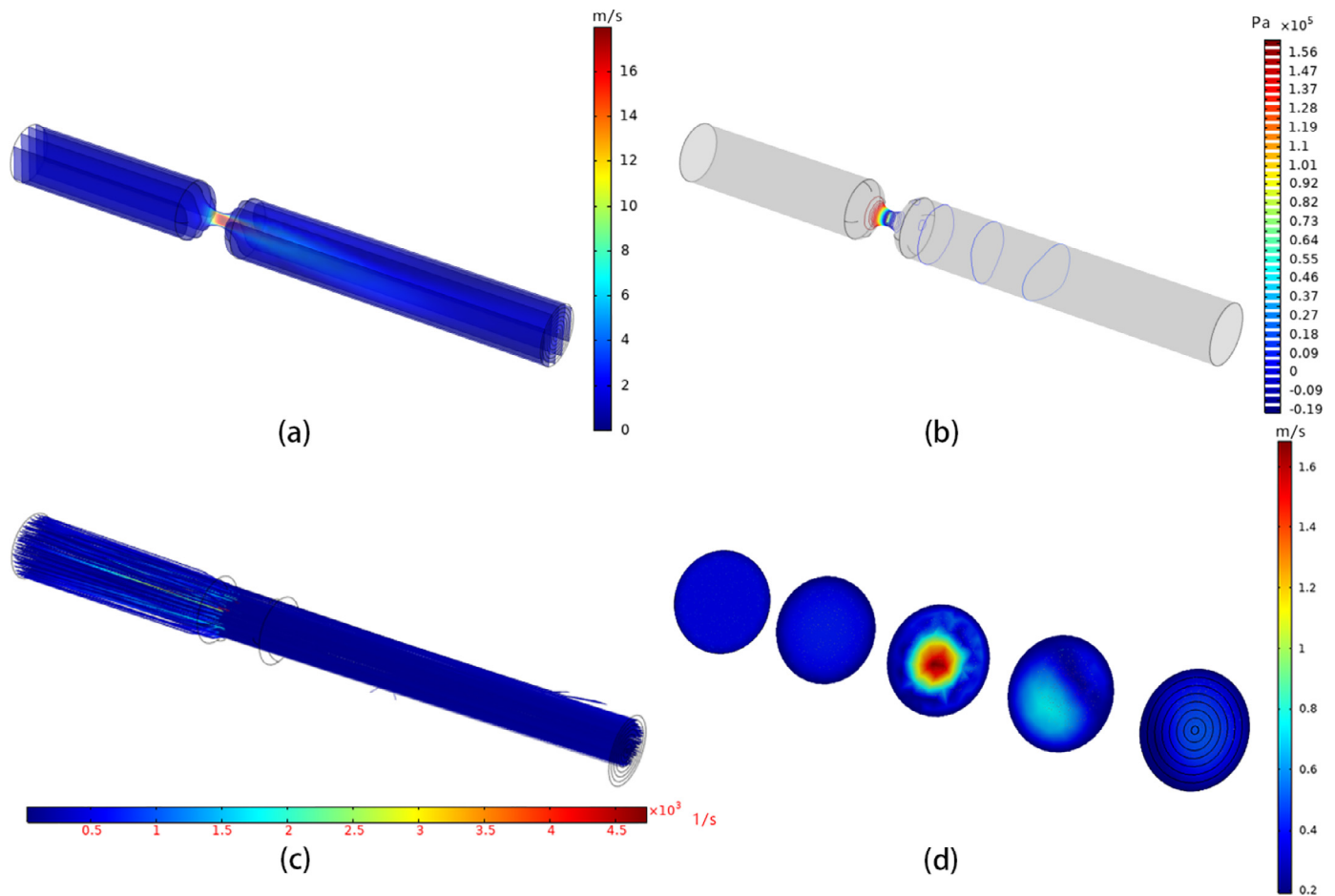


Fig. 13. (a) The fluid velocity, (b) the wall pressure, (c) the particle trajectory and (d) the Poincaré Map at 75% ASD.

boundary condition, the NPs keep the position when the instant strikes the wall. In addition, the fluid velocity would slow down when near the inner wall of the protrusion so that some NPs cannot reach the outlet in the simulation time.

The Poincaré map is defined as a mapping from Poincaré cross-section S , which is surface section transversal to the flow, to itself obtained by the trajectories from one intersection of the Poincaré cross-section S to the next [31]. A color point is generated where each particle passes through the Poincaré cross-section S . All distributions of a single NP trajectory on the Poincaré section S could find the points with the same distribution value in phase space. Consequently, Poincaré maps help visualize particle trajectories and deepen comprehension of NP motion near periodic solutions in NP dynamical systems. As shown in Fig. 9, five Poincaré cross-sections reveal the NP distribution at early-stage atherosclerosis. The continuous trajectories spread into discrete cross-sections, where the colors of each point indicate the frequency of the NPs passing through that point. All piercings performed by a single particle trajectory on the plane find points with the same distribution value in the phase space. A single Phase Portrait gives a snapshot of all particles simultaneously, whereas the Poincaré Map shows the intersection points of particles with a surface, even if these intersections occur at different times. All crossings of a single particle trajectory on the plane find points with the same distribution value in space. The Cut Plane data set could easily define a single Poincaré section or multiple parallel planes. In this paper, the invariant set of the Poincaré map is the distribution function, which is regarded as the probability of particles appearing on the cross-section.

The transmission arrival probability is defined as the ratio of the number of NPs arrived at the outlet section to the total number of NPs released. Some NPs will pass through the vessel over time, while the rest NPs stuck at the narrow site or adhere to the vessel wall for a long time. During the test time, it will not account for these non-arrival NPs. Table 2 shows the probabilities of NP arrival with ASD ranging from 5% to 60%. When ASD reaches 60%, the probability is too small to be observed. However, these data can still reflect the development of early-stage atherosclerosis.

Passing through the stenosis reshapes the bloodstream into a jet. While ASD is between 40% and 60%, the jet length would be maximum. When ASD reaches 60%, the intravascular environment becomes more complicated. The boundary layer separates from the vessel wall, flowing back to form a vortex. Further, when ASD reaches 80%, the jet flow length would become shorter and turn into a turbulent flow [28]. When ASD exceeds 60%, the vascular fluid gradually changes into a turbulent flow. The NP detection probability under 60% ASD is too small to distinguish. Hence, an altered model predicts ASD between 60% and 80%.

In the new model, the distance from the stenosis to the outlet ranges from 80 mm to 115 mm, and the detection position adjusts to the vessel centre with a radius of 5 mm. Figs. 10–13 show a comparison of the vessels when ASD ranges from 60% to 80%. In the previous situations, the NP velocity increases in the stenotic part, caused by the spray structure in the stenotic part according to the law of mass conservation. In addition, according to the Bernoulli equation, the velocity increase in the stenotic part is nec-

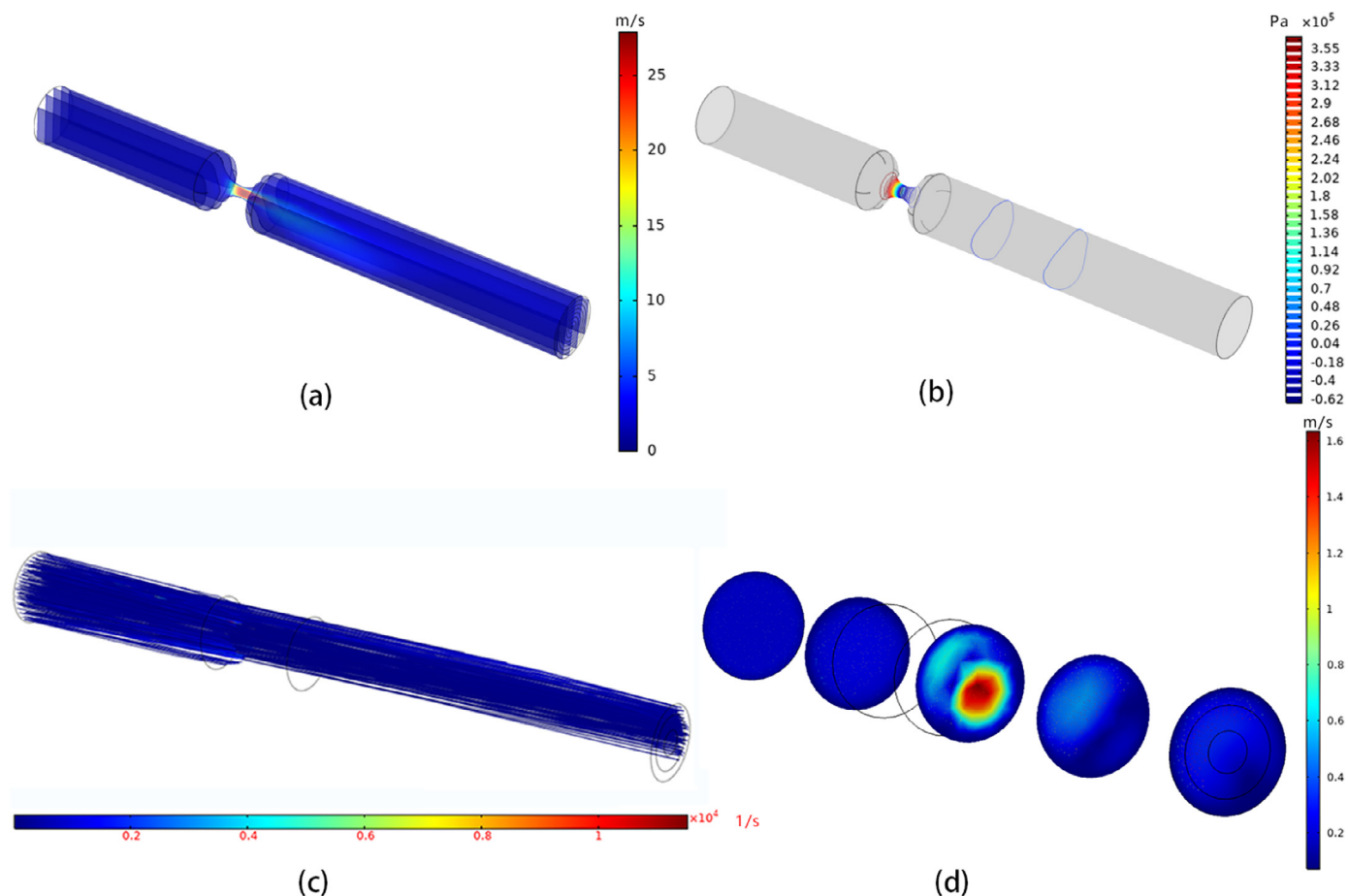


Fig. 14. (a) The fluid velocity, (b) the wall pressure, (c) the particle trajectory and (d) the Poincaré Map within a laminar flow at 80% ASD.

essarily accompanied by the pressure decrease. The NP shear velocity and pressure of the vessel wall still increase with the development of the stenosis. Therefore, the detection area is located at the centre position of the outlet, 185 mm away from stenosis, and the number of the detected particles still increases. In the advanced stage of atherosclerosis, ASD could reach 70%, the blood flux is largely reduced through the vessel, and most NPs cannot pass through the stenosis smoothly.

With increased vascular stenosis, the pressure of the larynx decreases more and more significantly, and it may even cause the blood vessel to collapse. In places farther away from the stenosis of the blood vessel, more severe stenosis may cause eddies and turbulence.

The NP detection probabilities with different levels of stenosis are shown in Table 3. In 60%-70% ASD, as the impulse of blood flow increases at the stenosis, the NP detection probability increases accordingly. At 75% ASD, the blood vessel is blocked, resulting in reducing NPs received. Figs. 14 and 15 show the comparison between the laminar and the turbulent fluid models at 80% ASD. It can be found that the NP detection probability is close to 0, which indicates the formation of turbulence. Whilst the turbulent flow forms, the corresponding flow velocity and wall pressure, are lower than those in the laminar flow. In addition, NPs motion is more stochastic, reducing the probability of reaching the detection site in simulation time.

From the data in Tables 2 and 3, it can be seen that as the ASD increases, that is, the cross-sectional area of the blood vessel through which the NPs pass decreases, the probability of ar-

rival NPs at the exit decreases, however, the change of discrete data is not linear. Fitting curves shown As shown in Fig. 16, according to discrete NP arrival probabilities corresponding to 5% to 60% of ASD. The overall curve shows a downward trend but not monotonously decreasing, and the slope of the probabilities fitting curve, namely the sensitivity, can be seen more intuitively according to Fig. 16. Similarly, the detection arrival probability of ASD from 60% to 80% refers to phase transition from laminar flow to turbulence, as shown in Fig. 17. We can find that the slope of the fitting curve is in an accelerated descent, which reveals a more rapid decline in NP arrival probability as ASD grew from 60% to 80%.

At the same time, there is a reflex area existing downstream of the stenosis. Due to the lack of material exchange, the oxygen and nutrient supply in the blood is insufficient, which inhibition or even pathological change of the functionality of the vessel wall. On the other hand, the frontal reticular structure composed of lipids and fibrin will be directly incorporated or attached to the surface of the blood vessel wall, causing pathological changes in the blood vessel wall.

The turbulence, characterized by irregular motion and energy loss, may cause cardiac overload. Moreover, the turbulence is likely to rupture red blood cells and causes hemolysis, thereby activating platelets. Once activated platelets enter the reflux, they would adhere to the vessel wall for a long time, activating other platelets encountered. A thrombus is formed with platelets, which would gradually become more prominent and eventually block the blood vessels.

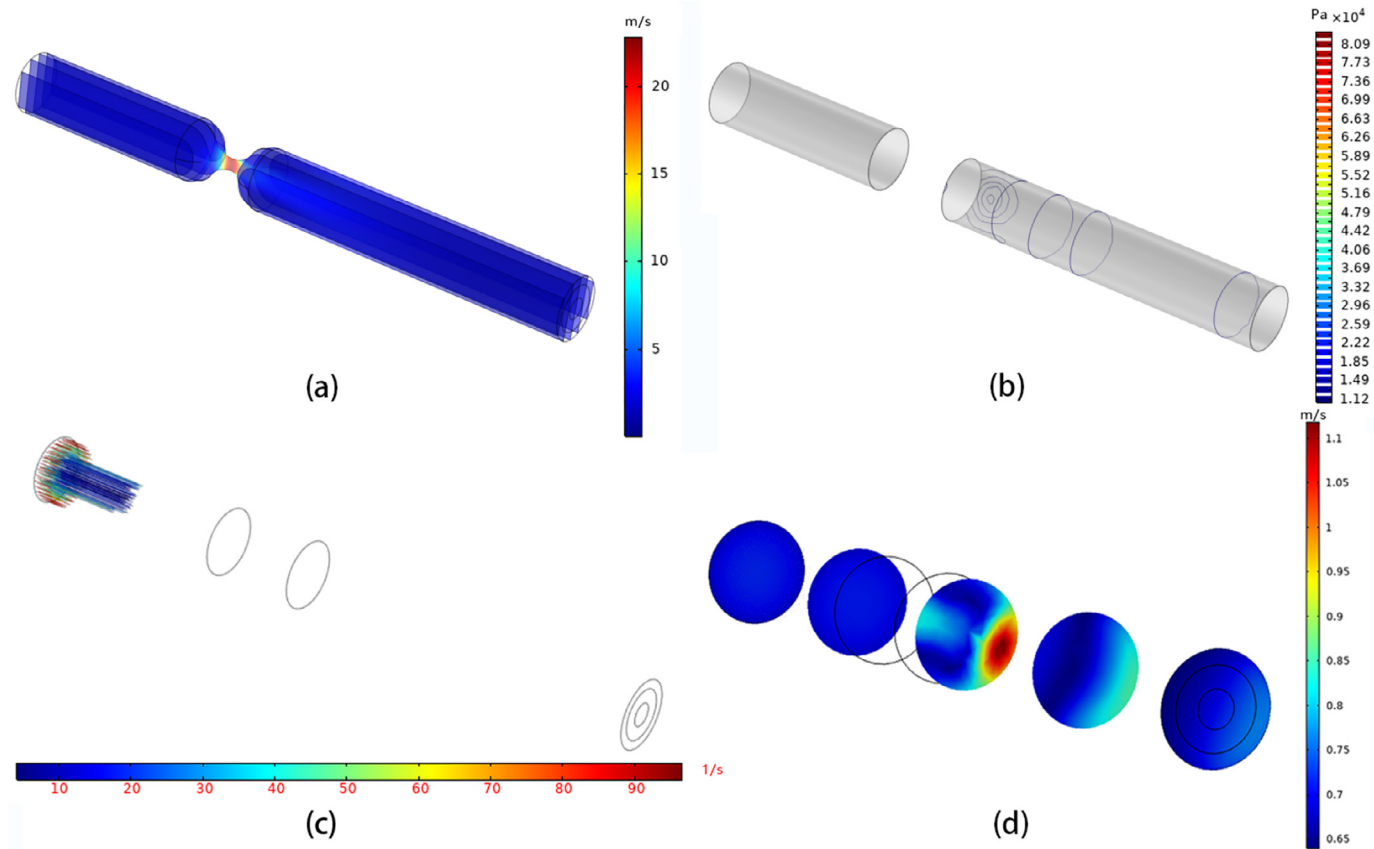


Fig. 15. (a) The fluid velocity, (b) the wall pressure, (c) the particle trajectory and (d) the Poincaré Map within a turbulent flow at 80% ASD.

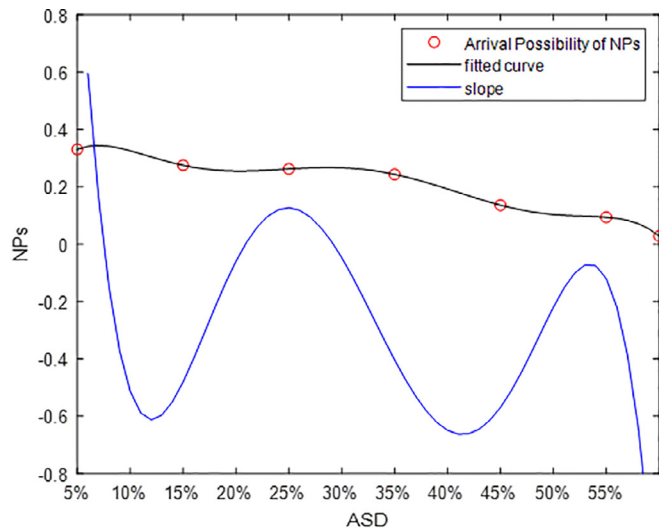


Fig. 16. A fitting curve of the discrete NP arrival probabilities corresponding to 5% to 60% of ASD and the slope of its fitting curve.

5. Discussion

In this paper, quantitative detection of the degree of atherosclerosis is achieved from the perspective of MC with the aid of existing medical imaging techniques, namely, angiography. In addition, an MC-based detection method is established by increasing ISI, which contributes to the early prediction of atherosclerosis. The method presented here can quantify the degree of lesions at vari-

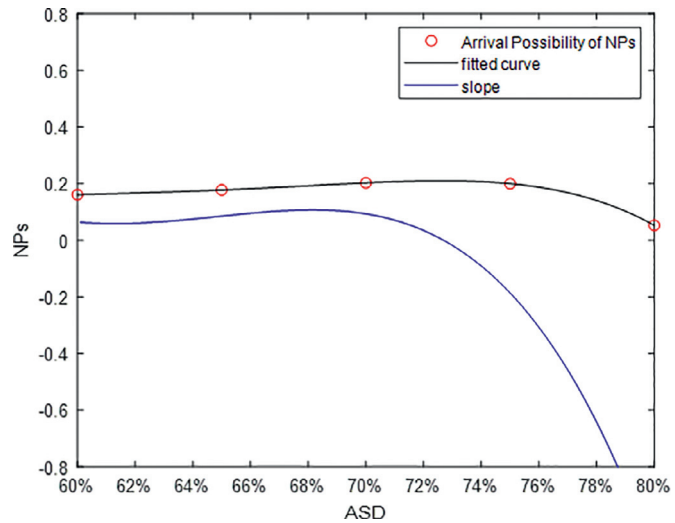


Fig. 17. A fitting curve of the discrete NP arrival probabilities corresponding to 60% to 80% of ASD and the slope of its fitting curve.

ous stages using direct data and is, therefore, more efficient, convenient, and accurate. If the ISI method is not introduced, it is difficult to distinguish the probability of exit detection in the early stage of blocking, as 5%–35% shown in the table below:

And if the entire section is directly used as the detection position, there will be indistinguishable results, as 5%–25% shown in the following table (Table 5):

In previous detection methods of vascular diseases, the personal experience of doctors is inevitably needed in the detection process.

If the data-driven method is adopted, it will undoubtedly help doctors and save labour costs. It should be noted that the above data is based on simple pipes with regular geometric shapes, but the actual three-dimensional structure of the stenosis vessel model and vessel composition parameters are complicated. Furthermore, the non-periodicity of blood flow would influence local hemodynamic parameters, [32] suggest that considering the non-periodic characteristic of blood flow could be important for studying hemodynamics in arteries with an enormous velocity or specific morphological characteristics. The accurate location of stenosis will be predicted under more complicated vascular conditions in the future.

Declaration of Competing Interest

We declare that we have no financial and personal relationships with other people or organizations that can inappropriately influence our paper, there is no professional or other personal interest of any nature that could be construed as influencing the position presented in the manuscript entitled.

References

- [1] World Health Organization, Media Centre: Cardiovascular Disease, World Health Organization, 2017. <http://www.who.int/mediacentre/factsheets/fs317/en/>.
- [2] J. Bejarano, et al., Nanoparticles for diagnosis and therapy of atherosclerosis and myocardial infarction: evolution toward prospective theranostic approaches, *Theranostics* 8 (17) (2018) 4710–4732.
- [3] E.J. Benjamin, et al., Heart disease and stroke statistics–2017 update: a report from the american heart association, *Circulation* 18 (2) (2017).
- [4] G.A. Roth, G.A. Mensah, V. Fuster, The global burden of cardiovascular diseases and risks, *J. Am. Coll. Cardiol.* 76 (25) (2020) 2980–2981.
- [5] Y. Uchida, E. Shimoyama, N. Hiruta, T. Tabata, Detection of early stage of human coronary atherosclerosis by angioscopic imaging of collagen subtypes, *J. Cardiol.* (2020).
- [6] J. Sanz, Z.A. Fayad, Imaging of atherosclerotic cardiovascular disease, *Nature* 451 (2008) 953–957.
- [7] S. Shepherd, K. Cadwallader, T.A. Jankowski, Does early detection of suspected atherosclerotic renovascular hypertension change outcomes? *J. Fam. Pract.* 54 (9) (2005) 9–12.
- [8] L. Dobnikar, et al., Disease-relevant transcriptional signatures identified in individual smooth muscle cells from healthy mouse vessels, *Nat. Commun.* 9 (1) (2018).
- [9] F. Hyafil, Noninvasive detection of macrophages using a nanoparticulate contrast agent for computed tomography, *Nat. Med.* (2007).
- [10] M. Nahrendorf, Nanoparticle PET-CT imaging of macrophages in inflammatory atherosclerosis, *Circulation* (2008).
- [11] R.K. Roeder, et al., Nanoparticle imaging probes for molecular imaging with computed tomography and application to cancer imaging, in: *Medical Imaging 2017: Physics of Medical Imaging*, 2017.
- [12] Y. Sun, R.Z. Zhang, Y. Chen, A molecular communication detection method for the deformability of erythrocyte membrane in blood vessels, *IEEE Trans. Nanobioscience* (2021) 1–9.
- [13] Y. Fang, W. Guo, M. Icardi, A. Noel, N. Yang, Molecular information delivery in porous media, *IEEE Trans. Mol. Biol. Multi-Scale Commun.* 4 (4) (2018) 257–262, doi:[10.1109/TMBMC.2019.2937297](https://doi.org/10.1109/TMBMC.2019.2937297).
- [14] W. Wicke, T. Schwering, A. Ahmadzadeh, V. Jamali, A. Noel, R. Schober, Modeling duct flow for molecular communication, in: *2018 IEEE Glob. Commun. Conf. GLOBECOM 2018 - Proc.*, 2018, pp. 206–212.
- [15] J.P. Mejia, Evaluation of wall shear stress in stent design: development of performance metrics, constitutive modelling, and experimental validation, McGill University, 2012 PhD thesis.
- [16] K.B. Manning, Biofluid mechanics: the human circulation, in: *Cardiovascular Engineering & Technology*, vol. 3, second ed., 2012, pp. 351–352.
- [17] N.J. Quinlan, P.N. Dooley, Models of flow-induced loading on blood cells in laminar and turbulent flow, with application to cardiovascular device flow, *Ann. Biomed. Eng.* 35 (8) (2007) 1347–1356, doi:[10.1007/s10439-007-9308-8](https://doi.org/10.1007/s10439-007-9308-8).
- [18] K. Iwamoto, N. Kasagi, Y. Suzuki, Direct numerical simulation of turbulent channel flow at Reynolds 2320, *Symp. Smart Control Turbul.* (327) (2005) 327–333.
- [19] Y.I. Cho, K.R. Kensey, Effects of the non-newtonian viscosity of blood on flows in a diseased arterial vessel. Part 1: steady flows, *Biorheology* 28 (3–4) (1991) 241–262, doi:[10.3233/BIR-1991-283-415](https://doi.org/10.3233/BIR-1991-283-415).
- [20] M. Rafiee, M.J.H. Simmons, A. Ingram, E.H. Stitt, Development of positron emission particle tracking for studying laminar mixing in Kenics static mixer, *Chem. Eng. Res. Des.* 91 (11) (2013) 2106–2113, doi:[10.1016/j.cherd.2013.05.022](https://doi.org/10.1016/j.cherd.2013.05.022).
- [21] T.W. Secomb, *Hemodynamics, Compr. Physiol.* 6 (2) (2016) 975.
- [22] C. Baker, et al., Computational techniques, in: *Train Aerodynamics, Butterworth-Heinemann*, 2019, pp. 53–71.
- [23] S.E. Rittgers, M.C.S. Shu, Doppler color-flow images from a stenosed arterial model: interpretation of flow patterns, *J. Vasc. Surg.* 12 (5) (1990) 511–522, doi:[10.1016/0741-5214\(90\)90002-R](https://doi.org/10.1016/0741-5214(90)90002-R).
- [24] K.B. Chandran, S.E. Rittgers, A.P. Yoganathan, *Biofluid Mechanics: The Human Circulation*, first ed., CRC Press, 2006, doi:[10.1201/9781420007213](https://doi.org/10.1201/9781420007213).
- [25] Y. Chahibi, M. Pierobon, S.O. Song, I.F. Akyildiz, A molecular communication system model for particulate drug delivery systems, *IEEE Trans. Biomed. Eng.* 60 (12) (2013) 3468–3483, doi:[10.1109/TBME.2013.2271503](https://doi.org/10.1109/TBME.2013.2271503).
- [26] L.L.M. Heaton, E. López, P.K. Maini, M.D. Fricker, N.S. Jones, *Advection, diffusion, and delivery over a network*, *Phys. Rev. E* 86 (2012) 021905–1–021905–10.
- [27] A.K. Datta, *Biological and Bioenvironmental Heat and Mass Transfer*, CRC Press, 2002.
- [28] B.D. Birch, *Hemodynamics. Second edition*, *Yale J. Biol. Med.* 62 (1) (1989) 50–51.
- [29] W. Wang, D. Yang, Y. Lu, Modeling and simulation of artery occlusion for early detection of carotid atherosclerosis, in: *2020 Chinese Control And Decision Conference (CCDC)*, 2020, pp. 4948–4952, doi:[10.1109/CCDC49329.2020.9164358](https://doi.org/10.1109/CCDC49329.2020.9164358).
- [30] E.J. Benjamin, et al., Heart disease and stroke statistics–2017 update: a report from the american heart association, *Circulation* 135 (10) (2017), doi:[10.1161/CIR.0000000000000485](https://doi.org/10.1161/CIR.0000000000000485).
- [31] G. Bertotti, I.D. Mayergoyz, C. Serpico, Dissipative magnetization dynamics, *Nonlinear Magn. Dyn. Nanosyst.* (2009) 91–126, doi:[10.1016/B978-0-08-044316-4.00007-4](https://doi.org/10.1016/B978-0-08-044316-4.00007-4).
- [32] X. Zhou, et al., Non-periodicity of blood flow and its influence on wall shear stress in the carotid artery bifurcation: an in vivo measurement-based computational study, *J. Biomech.* 101 (2020) 109617.